Research on a Highly Overmoded Slow Wave Circuit for 0.3-THz Extended Interaction Oscillator

Yifan Zu, Ying Lan, Xuesong Yuan, Xiaotao Xu, Qingyun Chen, Hailong Li, *Member, IEEE*, Matthew T. Cole, *Senior Member, IEEE*, Yong Yin, *Member, IEEE*, Bin Wang, Lin Meng, and Yang Yan

***Abstract*— Here, we present the complete design process of a highly overmoded slow wave circuit (SWC) stably operating in the quasi-TM_{04} mode for terahertz (THz) extended interaction oscillator (EIO). The developed interaction circuit emits THz frequency electromagnetic radiation through structural size of the engineered millimeter-wave (MMW) circuits, which provides a new technological horizon for overcoming the engineering challenges caused by the limitation of circuit size. Through careful engineering of the electron optical system, a cylindrical beam with a diameter of 0.38 mm and a current of 0.25 A is obtained at a bias of 14.8 kV. Through the particle-in-cell (PIC) simulation, these new design approaches have been shown to achieve an output power of 250 W at 0.3 THz in a cylindrical cavity with an inner diameter of 4.16 mm.**

***Index Terms*— Extended interaction oscillator (EIO), overmoded, slow wave circuit (SWC), terahertz (THz), vacuum electronics.**

I. Introduction

THE development of new microfabrication and nanofabrication technologies, aided by advances in computer-aided design and materials science, has ignited a renewed interest in the search for new types of mobile, high-power sources of electromagnetic radiation with emission peaks from millimeter wave (MMW) to the terahertz (THz) [1], [2]. Slow wave devices, such as traveling-wave tubes (TWTs), backward-wave oscillators (BWOs), and extended interaction devices (EIDs), have much development potential in military and commercial applications that require high frequency (HF) and high power due to their compact structure, high performance, and limited need for strong magnetic fields [3], [4], [5], [6], [7], [8]. However, due to coherent effects between frequency and feature size, challenges linked to the necessarily small circuit sizes as the frequency progresses to THz band cannot be ignored [9], [10], [11]. Recently, the reported slow wave structure (SWS) of folded-waveguide TWT operating above 0.3 THz has been reduced in transverse size to 0.51 mm, and the diameter of the beam tunnel is only 0.18 mm [12]. With the dramatic shrinking of transverse dimensions, device output power and stability are limited by factors such as the more laborious design of precisely aligned high-density electron beam, and more difficult engineering of machining and assembly.

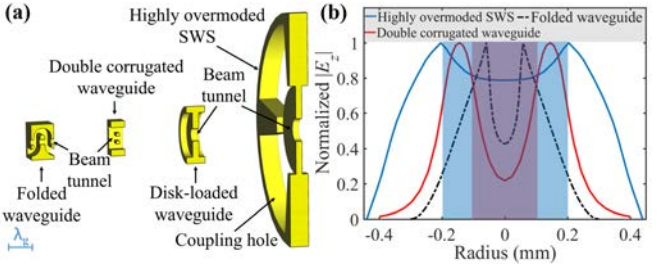

Fig. 1. Comparison of typical SWSs. (a) Schematic of the folded waveguide, the double corrugated waveguide, the disk-loaded waveguide, and the proposed highly overmoded SWS at the same frequency. (b) Normalized $|E_z|$-field distribution of the highly overmoded SWS, the folded waveguide, and the double corrugated waveguide on the beam tunnel section at the same frequency band.

In the typical several full-metal SWSs, as shown in Fig. 1(a), when the structural size of the circuit is severely restricted, it is not anticipated that the HF system operating in the conventional fundamental mode will be sufficient due to the equivalence of operating wavelength (λ_g). Compared with the commonly used fundamental mode, the most significant feature of the higher order mode is that it can support a physically larger interaction system for a given frequency, so as to enlarge the power capacity [13]. At present, extensive studies of sheet beam and multibeam have also largely provided valuable contributions to overcome the power limitations of devices, even demonstrating exciting performance in studies

Manuscript received 3 September 2022; revised 12 November 2022 and 24 January 2023; accepted 20 February 2023. Date of publication 9 March 2023; date of current version 24 March 2023. This work was supported in part by the National Key Research and Development Program of China under Grant 2019YFA0210202, in part by the Sichuan Science and Technology Program under Grant 2021YJ0096, and in part by the National Natural Science Foundation of China under Grant 61771096. The review of this brief was arranged by Editor L. Kumar. *(Corresponding author: Xuesong Yuan.)*

Yifan Zu, Xuesong Yuan, Xiaotao Xu, Qingyun Chen, Hailong Li, Yong Yin, Bin Wang, Lin Meng, and Yang Yan are with the Terahertz Science and Technology Key Laboratory of Sichuan Province, School of Electronic Science and Engineering, University of Electronic Science and Technology of China, Chengdu 610054, China (e-mail: yuanxs@uestc.edu.cn).

Ying Lan is with the Chengdu University of Traditional Chinese Medicine, Chengdu 611137, China (e-mail: lanyingmailbox@163.com).

Matthew T. Cole is with the Department of Electronic and Electrical Engineering, University of Bath, BA2 7AY Bath, U.K. (e-mail: m.t.cole@bath.ac.uk).

Color versions of one or more figures in this article are available at https://doi.org/10.1109/TED.2023.3249138.

Digital Object Identifier 10.1109/TED.2023.3249138

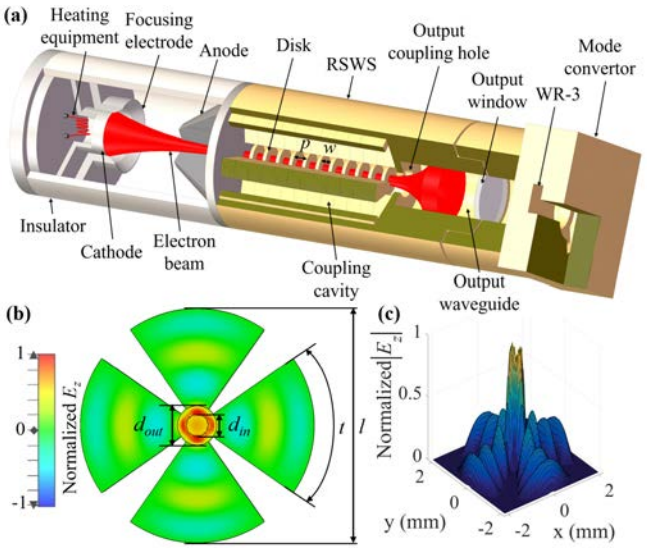

Fig. 2. Schematic depiction of a 0.3-THz EIO based on the highly overmoded structure. (a) 3-D model. (b) E_z-field distribution. (c) $|E_z|$-field contour plots of the quasi-TM_{04} mode at $z = 0$ plane.

combined higher order modes [14], [15], [16], [17]. However, due to the more difficult beam compression and transmission and the complex engineering of the focusing system, most of the reports are only simulation studies. It has also been noted that higher mode field distributions may result in a relatively weak beam–wave coupling, which poses unique challenges for improving efficiency and suppressing mode competition [18].

In this brief, we develop a novel technique that relies on engineering capabilities common in low-frequency bands to generate higher frequencies of electromagnetic radiation at larger circuit sizes. Insights gained using highly overmoded structures in the development of fast-wave devices are extended to slow wave circuits (SWCs) [19]. A specific extended interaction oscillator (EIO) design scheme is demonstrated, as shown in Fig. 2. The operation of a quasi-TM_{04} that is considered to have almost the same functional characteristics as the TM_{04} mode (the 40th in the circular waveguide) is established. Due to the realization of the method of concentrating the axial field energy along the source's central axis within a large cavity, an oversized beam tunnel that can support efficient energy conversion between the electron beam and the HF field is designed. As shown in Fig. 1(b), it was found that the beam tunnel diameter of the SWC operating in the quasi-TM_{04} mode can easily be increased to two times or more than that of the conventional SWCs, while the overall transverse dimension increases even more [12], [20]. Even with the same absolute error, the relative error of the designed highly overmoded structure is only half that of the traditional structure, which eases the engineering difficulty of processing and assembly. Furthermore, as the size of the beam tunnel increases, higher current electron beams can be employed, which directly increases the output power of the device.

II. Circuit and Components

Here, a design concept of the highly overmoded technique applied to SWCs is investigated. First, this design concept allows for a larger circuit size, which effectively mitigates engineering difficulties caused by fabrication and assembly. Second, from the Bessel function field, the higher

TABLE I
Design Parameters of 0.3-THz Circuit

Symbol	Description	Value and Unit
p	Period length	0.23 mm
w	Gap width	0.09 mm
d_{out}	Disk outer diameter	0.70 mm
d_{in}	Disk inner diameter	0.40 mm
l	Cavity inner diameter	4.16 mm
t	Coupling cavity angular width	70°
d_h	Output coupling hole diameter	0.78 mm
d_w	Output waveguide diameter	1.44 mm

the order of the TM_{0n} mode, the more concentrated the E_z-field strength in the beam tunnel, and the greater the interaction impedance [21]. In this way, even if the diameter of the beam tunnel is increased, the beam–wave coupling can also be maintained at a relatively high level. After preliminary empirical analysis, the quasi-TM_{04} mode is selected. A four-cavity loaded central ring structure that operates stably in the quasi-TM_{04} mode is developed, as shown in Fig. 2. The four fan-shaped coupling cavities have distributed axial symmetry, which not only increases the energy storage of the entire circuit but also indirectly adjusts the HF field distribution. The four pillars supporting the central metal ring divide the coupling cavity, thereby reducing the interference of most unwanted or additional modes on the operating mode. Moreover, the interaction area between electron and wave is compressed and concentrated near the metal ring to further enhance the axial field energy and improve the interaction impedance.

The design parameters of the highly overmoded SWC are given in Table I. The entire cavity inner diameter of this highly overmoded EIO is 4.16 mm, which is equivalent to the standard of conventional SWCs in the V-band or even the Ka-band [22], [23]. Here, a disk with a thickness of 0.23 mm is first processed into a single-period four-hole structure, and then, multiple disks are loaded into the sleeve to form an HF system, as shown in Fig. 2(a). We have verified the feasibility of related schemes in the reported development of BWO [24] and mode converter [25] and obtained high-performance indicators in the corresponding tests. Furthermore, we have fabricated a scale model at the Ka-band based on this four-cavity-loaded central ring structure, as shown in Fig. 3(a). The S-parameters of the structure were verified using a mode converter, as shown in Fig. 3(b) and (c). The quasi-TM_{04}-2π operating mode of the Ka-band scale model has been validated at 32.5 GHz. Also, its S_{11} parameter presents a more obvious negative peak in Fig. 3(b). By comparing the experimental results and simulation results, we find that the highly overmoded SWC produced by lower cost, medium-scale processing technology, and appropriate assembly conditions is capable of achieving the functional requirements of MMW circuits. Therefore, it is indirectly demonstrated that the larger circuit size designed by highly overmoded technology has great potential to alleviate the engineering challenges caused by higher frequencies.

The developed highly overmoded structure has provided a novel solution to circuit size limitations, but it may allow for multimode competition. Fig. 4(a) shows the dispersion characteristics of the circuit. The axial mode is planned as the 2π mode that provides a maximum electric field in the

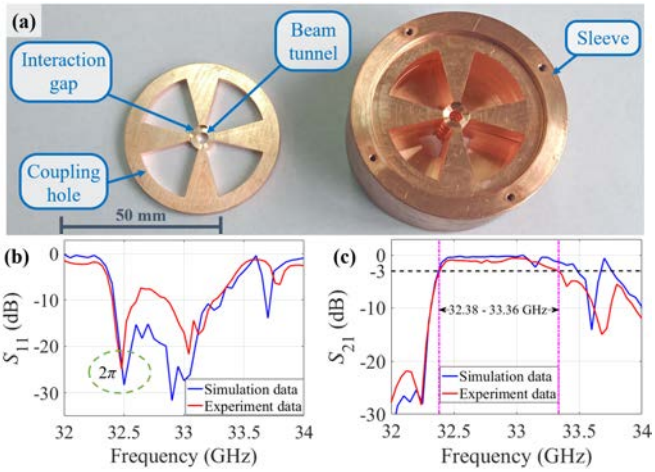

Fig. 3. Experiments to measure the transmission and oscillation properties of a scale model at *Ka*-band based on this highly overmoded structure. (a) Photograph of the manufactured components. Comparison of experimental and simulation results for (b) S_{11} and (c) S_{21} of the highly overmoded structure.

same direction on each gap. The quasi-TM_{03}, quasi-TM_{02}, and quasi-TM_{01} modes in the area near the intersection with the beam voltage line are considered to pose a competitive risk to the operating mode. Fig. 4(b) shows the physical parameters for these four modes, where R/Q is the characteristic impedance for evaluating the beam–wave coupling performance and Q_e and Q_0 are the external quality factor caused by diffraction loss and the intrinsic quality factor caused by ohmic loss, respectively [26]. As an important theoretical basis for judging the stable operation of a device, the start-oscillation criterion has been widely studied [27], [28]. When the dc energy of the electron beam is converted into HF field energy and the HF field energy is steadily increased, this defines the start of oscillatory behavior. The energy exchange between the electron beam and the operating mode field is usually expressed by the beam-load conductance G_e [18], [29], [30], [31], which is expressed as

$$G_e = \frac{1}{8}\frac{\beta_e}{\beta_q} G_0 \left[\left| M_-^2(\beta_e - \beta_q) \right| - \left| M_+^2(\beta_e + \beta_q) \right| \right] \quad (1)$$

where β_e and β_q represent the propagation constants of the dc electron beam and the reduced plasma, respectively [32], [33]. G_0 represents the dc conductance of the electron beam. $M_-(\beta_e - \beta_q)$ and $M_+(\beta_e + \beta_q)$ represent the coupling coefficients of fast and slow space charge waves, respectively, as follows [31]:

$$M_\pm(\beta_e \pm \beta_q) = \frac{\int_{-\infty}^{\infty} E(z) e^{j(\beta_e \pm \beta_q)z} dz}{\int_{-\infty}^{\infty} |E(z)| dz} \quad (2)$$

where $E(z)$ is the axial electric field distribution at the interaction gaps. Negative G_e suggests that the dc energy of the electron beam is being converted into HF field energy, which will be the prerequisite for oscillation commencement. Generally, g_e is used to represent the ability to transfer energy from the electron beam to the circuit, where $g_e = G_e/G_0$ [18]. Fig. 4(c) shows the change of the normalized g_e with the dc voltage of the electron beam. The quasi-TM_{04} mode has been shown to operate stably without interference from lower order spurious modes when the operating voltage is set between the relatively large working range of 14.5–15.2 kV.

Here, to match the proposed highly overmoded circuit, an electron optical system with a typical structure is designed. Fig. 5(a) shows a cross section depiction of the entire electron gun. The scheme of the permanent magnet focusing system is shown in Fig. 5(b) and (c). The magnetic material is samarium cobalt. During operation of the electron gun, electrons are thermally emitted through a heated filament. These electrons enter the beam tunnel under the acceleration of the anode after being compressed by the electrostatic field and the focusing magnetic field. The electron beam cross section is compressed from the cathode emission area of 0.403π mm^2 into a beam spot of approximately 0.036π mm^2. A small ripple electron beam with a maximum envelope diameter of 0.38 mm and a current of 0.25 A is obtained at a bias of 14.8 kV.

Although the designed quasi-TM_{04} mode SWC can directly generate the circular TM_{01} mode radiation output through aperture diffraction, considering the investigation of the oscillation characteristics of the highly overmoded structure, it is necessary to design a mode conversion circuit that can be practically tested. Based on our previously developed mode converter prototype [25], a circular TM_{01} to rectangular TE_{10} mode converter is designed. The rectangular waveguides are standard commercial WR-3 waveguides. Fig. 6(a) shows the simulated S_{11} parameter obtained at the standard rectangular waveguide port by accessing the mode converter. The desired quasi-TM_{04}-2π operating mode is confirmed on the S_{11} curve as a peak of –20 dB at 299.52 GHz. Fig. 6(b) shows the conversion efficiency of the mode converter. The bandwidth of $S_{21} \geq -1$ dB is 21.25 GHz from 284.95 to 306.22 GHz.

III. Circuit Performance Evaluation

To verify the holistic performance of the developed highly overmoded THz EIO, particle-in-cell (PIC) simulations are carried out for the interaction circuit. A cylindrical electron beam with a current of 0.25 A is injected into the highly overmoded resonant slow wave structure (RSWS) at a bias voltage of 14.8 kV. Oxygen-free copper is used as the metal background material for the device with a conductivity of 2.4×10^7 S/m. An output power over 250 W is obtained, as shown in Fig. 7(a). The beam–wave interaction efficiency is about 6.7%. Fig. 7(b) shows the electron bunching in the cavity when the electron beam interacts with the quasi-TM_{04} mode field. The inset of Fig.7(b) shows the spectrum of the output signal. Fig. 7(c) shows the effect of the electron beam voltage on the output power, interaction efficiency, and operating frequency. The designed circuit is stably operated in the quasi-TM_{04} mode with a tuning frequency range of about 299.4–299.7 GHz. As shown in Fig. 8, the electron beam of 0.25-A current with 95% filling rate still has a beam transparency higher than 98% when the device operates stably and maintains an output power of 250 W.

We further considered the beam alignment error, electron angle spread, and electron energy spread that almost certainly exist due to real-world processing, to ensure a substantial evaluation of the performance and stability of the device. As shown in Fig. 9(a)–(c), the designed interaction circuit demonstrates moderate tolerance in terms of beam alignment error, electron emission angle spread, and electron energy

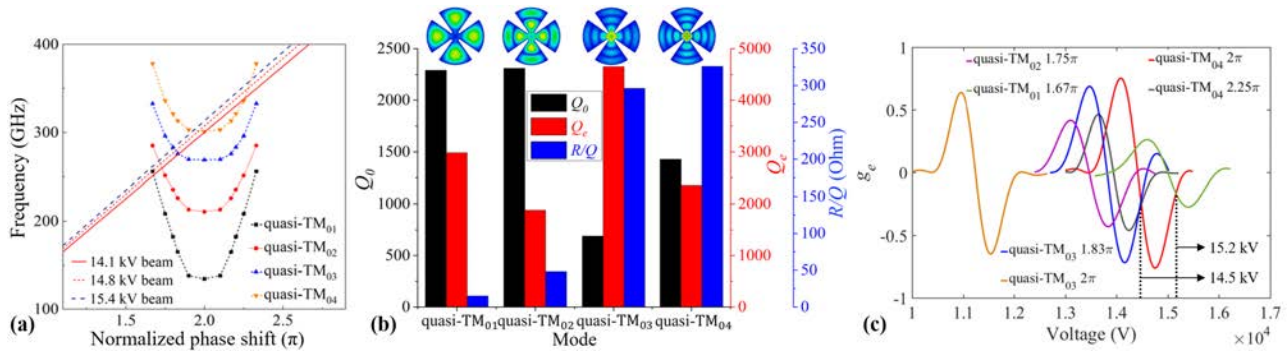

Fig. 4. Model competition analysis. (a) Dispersion diagram of the designed circuit. (b) Q_0, Q_e, and R/Q of the quasi-TM_{01} mode, quasi-TM_{02} mode, quasi-TM_{03} mode, and quasi-TM_{04} mode. (c) Normalized g_e variation with the electron beam voltage in the designed circuit.

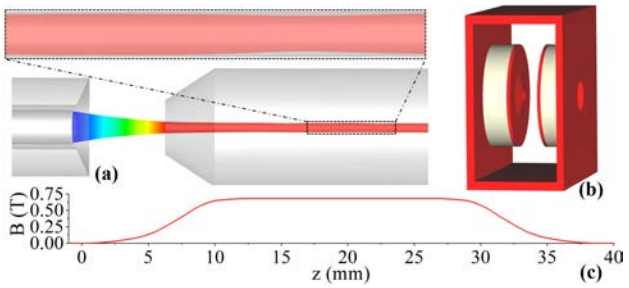

Fig. 5. Electron optical system preliminary design model. (a) Beam trajectory in the electron gun. (b) Simulation model of the permanent magnet. (c) Magnetic field intensity distribution of the permanent magnetic field on the axis.

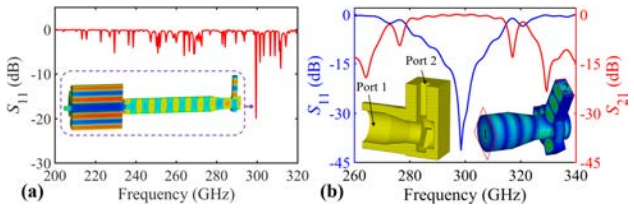

Fig. 6. Simulated cold test characteristics of the 0.3-THz EIO. (a) Typical S_{11} simulation results at the standard rectangular waveguide port. Inset: E_z-field distribution of the EIO at 299.52 GHz. (b) S-parameters of the mode converter. Insets: cross-sectional schematic of the mode converter, and the electric field distribution in the mode converter when TM_{01} is fed in port 1 and TE_{10} is output from port 2.

spread. Commonly, the reduced effective conductivity value to replace the extra ohmic loss due to surface roughness is used to integrate such effects into design activities. The correlation effect between effective conductivity and rough surface finish has been presented by Datta et al. [34] and Kirley et al. [35] in their study of conductivity loss analysis of structures. The following equation elaborates a proximate relationship between effective conductivity and surface roughness:

$$\sigma_{\text{eff}} = \frac{\sigma_{\text{ide}}}{\left(1 + \exp\left(-\left(\frac{s}{2h}\right)^{1.6}\right)\right)^2} \tag{3}$$

where σ_{eff} represents the effective conductivity and σ_{ide} is the conductivity of the metals having ideal surface. The ideal conductivity σ_{ide} of oxygen-free copper is 5.8×10^7 S/m. h is the surface roughness measured as a root-mean-square deviation of the surface from its mean planar position. s is the skin depth for the ideal metals, which is calculated from

$$s = \frac{1}{\sqrt{\pi f \mu \sigma}} \tag{4}$$

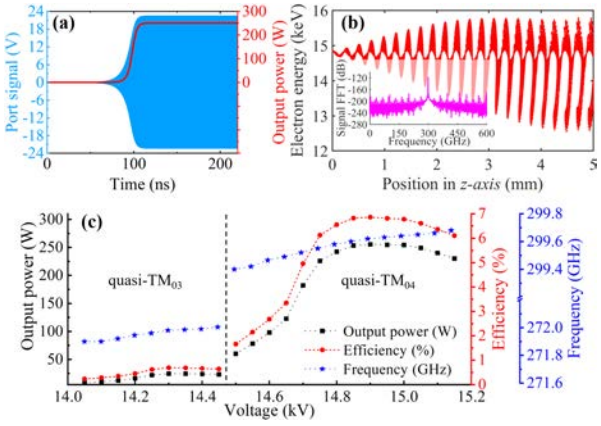

Fig. 7. PIC simulation verification of output power. (a) Output signal amplitude. (b) Phase-space diagram of electron energy. Inset: output signal spectrum. (c) Output power, frequencies, and the beam–wave interaction efficiency versus beam voltage.

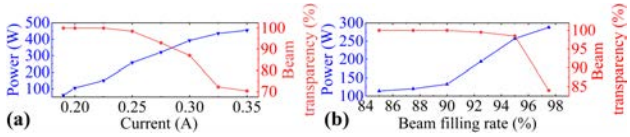

Fig. 8. Output power and beam transparency as a function of (a) beam current and (b) beam filling factor.

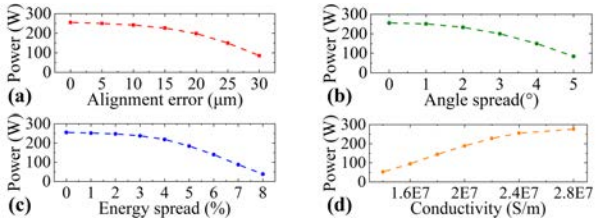

Fig. 9. Device tolerance evaluation. Effects of (a) electron beam alignment error, (b) electron angle spread, (c) electron energy spread, and (d) conductivity on the highly overmoded EIO output power.

where f is the operating frequency, μ is the magnetic permeability, and the value is a constant of $4\pi \times 10^{-7}$ H/m. The effective conductivity of copper decreases rapidly with increasing surface roughness when the surface roughness is on the order of the skin depth. This rapid decrease is followed by asymptotic behavior for very rough surfaces beyond the skin depth. With the continuous decrease in conductivity, increasing amounts of energy is lost in the cavity wall via ohmic heating. As shown in Fig. 9(d), this results in a continuous reduction in output power. Therefore, loss of conductivity

in the structure caused by rough surface finish is one of the limiting factors for device efficiency and average power handling capability. A number of approaches are worth trying here, such as providing a good surface finish to the structure and providing a coating of high conductivity on the surface of the material [36], [37].

IV. Conclusion

In this brief, we report on the holistic development of a new highly overmoded SWC that overcomes a variety of severe engineering challenges bought about by the growing demand for higher frequencies. A quasi-TM_{04} mode SWC for EIO that can generate 0.3-THz electromagnetic radiation with an output power of 250 W within a V-band standard cavity using a W-band size electron beam without requiring a superconducting magnetic system has been verified. Such new holistic design approaches achieve higher THz frequency electromagnetic radiation in the MMW circuit engineering.

References

[1] P. H. Siegel, "Terahertz technology," *IEEE Trans. Microw. Theory Techn.*, vol. 50, no. 3, pp. 910–928, Mar. 2002, doi: 10.1109/22.989974.

[2] J. H. Booske et al., "Vacuum electronic high power terahertz sources," *IEEE Trans. Terahertz Sci. Technol.*, vol. 1, no. 1, pp. 54–75, Sep. 2011, doi: 10.1109/TTHZ.2011.2151610.

[3] A. S. Gilmour and I. Ebrary, *Klystrons, Traveling Wave Tubes, Magnetrons, Crossed-Field Amplifiers, and Gyrotrons*. Norwood, MA, USA: Artech House, 2011.

[4] M. Sumathy et al., "Design and RF characterization of high-power ferrule-loaded folded waveguide SWS for mm-Wave TWT," *IEEE Trans. Plasma Sci.*, vol. 49, no. 11, pp. 3487–3493, Nov. 2021, doi: 10.1109/TPS.2021.3116615.

[5] V. L. Christie, L. Kumar, and N. Balakrishnan, "Inverted slot-mode slow-wave structures for traveling-wave tubes," *IEEE Trans. Microw. Theory Techn.*, vol. 55, no. 6, pp. 1112–1117, Jun. 2007, doi: 10.1109/TMTT.2007.897661.

[6] J. Feng et al., "Fabrication of a 0.346-THz BWO for plasma diagnostics," *IEEE Trans. Electron Devices*, vol. 65, no. 6, pp. 2156–2163, Jun. 2018, doi: 10.1109/TED.2018.2821683.

[7] D. Berry et al., "Practical aspects of EIK technology," *IEEE Trans. Electron Devices*, vol. 61, no. 6, pp. 1830–1835, Jun. 2014, doi: 10.1109/TED.2014.2302741.

[8] B. Steer, A. Roitman, P. Horoyski, M. Hyttinen, R. Dobbs, and D. Berry, "Advantages of extended interaction klystron technology at millimeter and sub-millimeter frequencies," in *Proc. 16th IEEE Int. Pulsed Power Conf.*, Jun. 2007, pp. 1049–1053, doi: 10.1109/PPPS.2007.4652369.

[9] S. Bhattacharjee et al., "Folded waveguide traveling-wave tube sources for terahertz radiation," *IEEE Trans. Plasma Sci.*, vol. 32, no. 3, pp. 1002–1014, Jun. 2005, doi: 10.1109/TPS.2004.828886.

[10] C. D. Joye et al., "Demonstration of a high power, wideband 220-GHz traveling wave amplifier fabricated by UV-LIGA," *IEEE Trans. Electron Devices*, vol. 61, no. 6, pp. 1672–1678, Jun. 2014, doi: 10.1109/TED.2014.2300014.

[11] N. Nayek, M. K. Joshi, R. K. Sonkar, T. Tiwari, and R. Bhattacharjee, "Design and analysis of width-modulated two-section sine waveguide for G-band traveling-wave tube," *IEEE Trans. Electron Devices*, vol. 68, no. 12, pp. 6458–6464, Dec. 2021, doi: 10.1109/TED.2021.3117894.

[12] P. Hu et al., "Demonstration of a watt-level traveling wave tube amplifier operating above 0.3 THz," *IEEE Electron Device Lett.*, vol. 40, no. 6, pp. 973–976, Jun. 2019, doi: 10.1109/LED.2019.2912579.

[13] D. Wang, G. Wang, J. Wang, S. Li, P. Zeng, and Y. Teng, "A high-order mode extended interaction klystron at 0.34 THz," *Phys. Plasmas*, vol. 24, no. 2, Feb. 2017, Art. no. 023106, doi: 10.1063/1.4975649.

[14] A. Bansiwal, S. Raina, K. J. Vinoy, and S. K. Datta, "A broadband rectangular reentrant cavity for multiple-beam klystron," *IEEE Trans. Electron Devices*, vol. 66, no. 7, pp. 3168–3170, Jul. 2019, doi: 10.1109/TED.2019.2916222.

[15] Y. Gong et al., "A 140-GHz two-beam overmoded folded-waveguide traveling-wave tube," *IEEE Trans. Plasma Sci.*, vol. 39, no. 3, pp. 847–851, Mar. 2011, doi: 10.1109/TPS.2010.2100410.

[16] J. Qing, X. Niu, T. Zhang, Y. Liu, G. Guo, and H. Li, "THz radiation from a TM_{51} mode sheet beam extended interaction oscillator with low injection," *IEEE Trans. Plasma Sci.*, vol. 50, no. 4, pp. 1081–1086, Apr. 2022, doi: 10.1109/TPS.2022.3155772.

[17] F.-M. Lin, S. Wu, Y. Xiao, and L. Zhang, "A 0.3 THz multi-beam extended interaction klystron based on $TM_{10,1,0}$ mode coaxial coupled cavity," *IEEE Access*, vol. 8, pp. 214383–214391, 2020, doi: 10.1109/ACCESS.2020.3040394.

[18] L. Bi et al., "Design and analysis of a high-order mode ladder-type RF circuit for stable operation in a W-band extended interaction oscillator," *IEEE Trans. Electron Devices*, vol. 66, no. 1, pp. 729–735, Jan. 2019, doi: 10.1109/TED.2018.2882956.

[19] R. K. Parker, R. H. Abrams, B. G. Danly, and B. Levush, "Vacuum electronics," *IEEE Trans. Microw. Theory Techn.*, vol. 50, no. 3, pp. 835–845, Mar. 2002, doi: 10.1109/22.989967.

[20] J. Zhang et al., "High energy beam THz backward wave oscillator based on double corrugated waveguide," in *Proc. IEEE Int. Vac. Electron. Conf. (IVEC)*, Apr. 2016, pp. 1–2, doi: 10.1109/IVEC.2016.7561911.

[21] D. M. Pozar, *Microwave Engineering*, 4th ed. New York, NY, USA: Wiley, 2011.

[22] M. Liao et al., "A novel folded waveguide for V-band TWT," *IEEE Trans. Plasma Sci.*, vol. 43, no. 12, pp. 4088–4091, Dec. 2015, doi: 10.1109/TPS.2015.2490119.

[23] C. Paoloni, M. Mineo, M. Henry, and P. G. Huggard, "Double corrugated waveguide for Ka-band traveling wave tube," *IEEE Trans. Electron Devices*, vol. 62, no. 11, pp. 3851–3856, Nov. 2015, doi: 10.1109/TED.2015.2480535.

[24] X. Yuan et al., "A carbon nanotube-based hundred watt-level Ka-band backward wave oscillator," *IEEE Trans. Electron Devices*, vol. 68, no. 5, pp. 2467–2472, May 2021, doi: 10.1109/TED.2021.3066144.

[25] Q. Chen et al., "Development of a Ka-band circular TM_{01} to rectangular TE_{10} mode converter," *IEEE Trans. Electron Devices*, vol. 67, no. 3, pp. 1254–1258, Mar. 2020, doi: 10.1109/TED.2020.2968347.

[26] A. Bansiwal, S. Raina, S. Datta, K. J. Vinoy, and S. K. Datta, "A simple method for estimating the quality factor of cylindrical re-entrant cavity of Klystrons," *J. Electromagn. Waves Appl.*, vol. 33, no. 8, pp. 1082–1091, Mar. 2019, doi: 10.1080/09205071.2019.1592710.

[27] S. K. Datta, L. Kumar, and B. N. Basu, "A simple closed-form formula for backward-wave start-oscillation condition for millimeter-wave helix TWTs," *Int. J. Infr. Millim. Waves*, vol. 29, no. 6, pp. 608–616, Jun. 2008, doi: 10.1007/s10762-008-9343-z.

[28] D. H. Preist and W. J. Leidigh, "Experiments with high-power CW Klystrons using extended interaction catchers," *IEEE Trans. Electron Devices*, vol. ED-10, no. 3, pp. 201–211, May 1963, doi: 10.1109/T-ED.1963.15176.

[29] R. J. Barker, J. H. Booske, N. C. Luhmann, and G. S. Nusinovich, "Klystrons," in *Modern Microwave and Millimeter-Wave Power Electronics*, 1st ed. Piscataway, NJ, USA: IEEE Press, 2005, pp. 131–147.

[30] Y. Ding, *Theory and Computer Simulation of High Power Klystron*. Beijing, China: National Defense Industry Press, 2008, pp. 44–47.

[31] X. Xu et al., "Design of a G-band extended interaction klystron based on a three-coupling-hole structure," *IEEE Trans. Electron Devices*, vol. 69, no. 3, pp. 1368–1373, Mar. 2022, doi: 10.1109/TED.2021.3138840.

[32] S. K. Datta and L. Kumar, "A simple closed-form formula for plasma-frequency reduction factor for a solid cylindrical electron beam," *IEEE Trans. Electron Devices*, vol. 56, no. 6, pp. 1344–1346, Jun. 2009, doi: 10.1109/TED.2009.2017649.

[33] G. M. Branch and T. G. Mihran, "Plasma frequency reduction factors in electron beams," *IRE Trans. Electron Devices*, vol. 2, no. 2, pp. 3–11, Apr. 1955, doi: 10.1109/T-ED.1955.14065.

[34] S. K. Datta, L. Kumar, and B. N. Basu, "A simple and accurate analysis of conductivity loss in millimeter-wave helical slow-wave structures," *J. Infr. Millim. THz Waves*, vol. 30, no. 4, pp. 381–392, Apr. 2009, doi: 10.1007/s10762-008-9455-5.

[35] M. P. Kirley, N. Carlsson, B. B. Yang, and J. H. Booske, "Study of the effect of surface roughness and skin depth on the conductivity of metals at 650 GHz," in *Proc. Int. Vac. Electron. Conf.*, Aug. 2012, pp. 239–240, doi: 10.1109/IVEC.2012.6262147.

[36] P. K. Jain and B. N. Basu, "The effect of conductivity losses on propagation through the helical slow-wave structure of a traveling-wave tube," *IEEE Trans. Electron Devices*, vol. ED-35, no. 4, pp. 549–558, Apr. 1988, doi: 10.1109/16.2494.

[37] A. S. Gilmour, M. R. Gillette, and J.-T. Chen, "Theoretical and experimental TWT helix loss determination," *IEEE Trans. Electron Devices*, vol. ED-26, no. 10, pp. 1581–1588, Oct. 1979, doi: 10.1109/T-ED.1979.19656.